Investigation of Electron Effective Mass in AlGaN/GaN Heterostructures by THz Spectroscopy of Drude Conductivity

Daniil Pashnev, Vadym V. Korotyeyev, Justinas Jorudas, Andrzej Urbanowicz, Pawel Prystawko, Vytautas Janonis, and Irmantas Kašalynas, *Senior Member, IEEE*

***Abstract*— Terahertz time domain spectroscopy (TDS) of the two-dimensional (2-D) electrons in various commercial AlGaN/GaN heterostructures was performed in the frequency range of 0.1–2.0 THz at selected temperatures of 80 and 300 K. Experimental transmission spectra were analyzed using analytical model derived for the thin conductive layer on dielectric substrate assuming a high-frequency Drude response of electrons. Two-dimensional electron mobility and density values found from the best fit parameters were compared with the results of independent Hall experiment demonstrating good agreement within uncertainty range of 10%. Thermal renormalization of the electron effective mass was revealed in all investigated samples manifesting as the increase of up to 1.45 ± 0.13 fold of nominal value obtained at cryogenic temperatures. Fast method based on measurement of the ratio of transmission spectra at two temperatures (80 and 300 K) was proposed to monitor the renormalization phenomenon in the samples with thin Drude conductivity layer where carrier density is relatively independent on temperature.**

***Index Terms*— AlGaN/GaN heterostructures, electron effective mass, terahertz time-domain spectroscopy (TDS), two-dimensional (2-D) electrons.**

Manuscript received March 7, 2022; revised April 28, 2022 and May 19, 2022; accepted May 19, 2022. Date of publication June 1, 2022; date of current version June 21, 2022. This work was supported in part by the Research Council of Lithuania (Lietuvos Mokslo Taryba) through the "T-HP" Project under Grant DOTSUT-184 funded by the European Regional Development Fund according to the supported activity "Research Projects Implemented by World-Class Researcher Groups" under Contract 01.2.2-LMT-K-718-03-0096 and in part by the National Centre for Research and Development of Poland under Grant WPC/20/DefeGaN/2018. The review of this article was arranged by Editor J. Mateos. *(Corresponding author: Irmantas Kašalynas.)*

Daniil Pashnev, Justinas Jorudas, Andrzej Urbanowicz, Vytautas Janonis, and Irmantas Kašalynas are with the Terahertz Photonics Laboratory, Center for Physical Sciences and Technology (FTMC), 02300 Vilnius, Lithuania (e-mail: daniil.pashnev@ftmc.lt; justinas.jorudas@ftmc.lt; andzej.urbanovic@ftmc.lt; vytautas.janonis@ftmc.lt; irmantas.kasalynas@ftmc.lt).

Vadym V. Korotyeyev was with the Terahertz Photonics Laboratory, Center for Physical Sciences and Technology (FTMC), 02300 Vilnius, Lithuania. He is now with the Department of Theoretical Physics, Institute of Semiconductor Physics, National Academy of Sciences of Ukraine (NASU), 03028 Kyiv, Ukraine (e-mail: vadym.korotieiev@ftmc.lt).

Pawel Prystawko is with the Institute of High Pressure Physics (UNIPRESS), Polish Academy of Sciences (PAS), 01-142 Warsaw, Poland (e-mail: pprysta@unipress.waw.pl).

Color versions of one or more figures in this article are available at https://doi.org/10.1109/TED.2022.3177388.

Digital Object Identifier 10.1109/TED.2022.3177388

I. Introduction

THIN conductive layers of the two-dimensional (2-D) electron gas (2DEG) in AlGaN/GaN heterostructures are widely used for the development of high electron mobility transistors (HEMTs) [1]–[4], high-frequency electronics, and terahertz (THz) photonics [5]–[8]. Rapid progress of such 2-D structures requires advanced noncontact characterization methods [9]. The THz time domain spectroscopy (TDS) allows simultaneous investigation of complex conductivity characteristics of the material by measurement of the amplitude and phase spectra in transmission and reflection geometries [10]. Usually Drude model of electron conductivity is employed for study of THz wave interaction with optically thin conductive layers [11]–[13]. A sophisticated transfer matrix method is widely used to describe spectra of multilayer samples [14], [15]. As an alternative, analytical equations of the transmission coefficient were derived by solving Maxwell equations for a two-component system composed of a thin conductive layer on a thick insulating substrate [16]. Applicability of these analytical equations to describe the high-frequency characteristics of 2DEG in a commercial AlGaN/GaN HEMT structure versus a transfer matrix method approach was recently demonstrated [17].

The electron effective mass, m^*, is an important basic parameter that defines the mobility of electrons and influences the speed of electronic device. Thermal renormalization of m^* was recently found in the AlGaN/GaN heterostructures using advanced experimental methods [15], [18]–[21]. Usually, the AlN spacer between the barrier and channel layers is used to localize 2DEG in a quantum well by minimizing the penetration of wave function into the barrier layer [22]. In very first experiments, the electron effective mass in $Al_{0.25}Ga_{0.75}N$/AlN/GaN on sapphire substrate at 300-K temperature was found to be similar to that in GaN material with value of about $m^* = 0.22m_e$ [23]. However in some $Al_xGa_{1-x}N$/AlN/GaN heterostructures on the SiC substrate, it was found to be significantly larger at room temperature than at cryogenic temperatures [15], [20], raising a question of whether the phenomenon is related to a specific sample or it is an intrinsic property of semiconductor devices, operation of which is based-on the Drude conductivity of 2DEG layer [13], [19], [24].

In this work, a THz-TDS of 2DEG conductivity in various commercial AlGaN/(AlN)/GaN HEMT structures was investigated aiming to reveal the influence of the AlN spacer to the renormalization phenomenon of m^* in nitride heterostructures. Modeling electron conductivity as [13]

$$\sigma_\omega = \sigma_{\rm dc}/(1 - i\omega\tau_{\rm sc}) \quad (1)$$

two important parameters Γ_e and γ_e were obtained after numerical analysis of the THz transmission spectra. Former describes the radiative decay rate, which is proportional to the ratio between the carrier density and the effective mass, n_e/m^*, while latter is the nonradiative decay rate associated with electron scattering time, $\tau_{\rm sc}$ [25]. The 2DEG density and mobility, $\mu_e = e/\gamma_e m^*$, were found from the analysis of THz spectra and the independent Hall measurements of low-field dc-conductivity, $\sigma_{\rm dc}$, employing a Van der Pauw structures fabricated in addition. Good agreement between experimental and numerical data as well as observed the decrease of Γ_e values with the increase of temperature allowed us to conclude that mass renormalization phenomenon is present in all heterostructures studied. Moreover, the contact-less method is proposed for characterization of Drude conductivity of the thin conductive layer on the dispersion-less substrate that requires neither external magnetic fields as for THz optical Hall effect measurements [26] nor grating-coupler for 2-D plasmon excitation in the heterostructure under research [27].

II. Results

Fig. 1 schematically illustrates the propagation of THz pulse through the sample, the layer design of which is sketched below indicating main differences between two groups of investigated samples. Standard commercial AlGaN/(AlN)/GaN HEMT structures on SiC substrate were kindly provided for the research by TopGaN (www.topganlasers.com) and SweGaN (www.swegan.se) companies. In total eight different HEMT structures were received, the number of which was limited by cost per wafer growth on a 4-in high-resistivity substrate. All samples were grouped as those without AlN spacer (F3 and M3) and with AlN spacer (C10, k9, D3, K11, J3, and #9) as schematically are shown in Fig. 1(a) and (b), respectively. To study the difference between conductive 2DEG layer and remaining nonconductive layers, one HEMT structure without AlN spacer (sample F3) was processed by removing selectively top layers down to GaN buffer in well-defined areas (zones) using a chlorine-based reactive ion etching (RIE) methods as described elsewhere [15]. The Hall effect experiments in Van der Paw geometry allowed us to obtain n_e and μ_e values of 2DEG in all samples at two temperatures of 77 and 300 K. Found values for selected F3 sample are summarized in a column "Hall" in Table I.

A commercial THz TDS system (TeraVil T-SPEC 800) was used to measure the transmission spectra in the frequency range of 0.1–2.0 THz at two selected temperatures. The THz pulses transmitted through the empty space (reference) and the substrate with heterostructure layers (sample) were recorded through a 3-mm-diameter aperture in a configuration of normal

TABLE I
Density and Mobility of 2DEG in F3 Sample

Parameter	Hall	THz TDS
μ(300 K), cm^2/V s	1864 ± 53	1576 ± 212
μ(80 K), cm^2/V s	18160 ± 1780	17744 ± 302
n_e(300 K) 10^{12}, cm^{-2}	9.27 ± 0.54	8.50 ± 0.97
n_e(80 K) 10^{12}, cm^{-2}	8.33 ± 0.48	7.65 ± 0.40

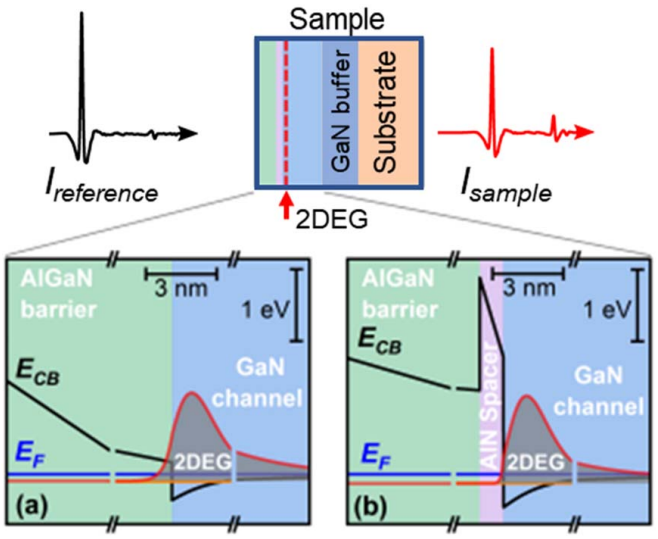

Fig. 1. Top line: Configuration of the experimental setup for THz transmission spectroscopy of Drude conductivity of 2DEG in the sample. Bottom line: Typical band diagram and 2DEG density profiles (red lines) in the heterostructures composed of AlGaN barrier and GaN channel (a) without and (b) with AlN spacer used for proper electron localization in a quantum well.

incidence. Fast Fourier transformation of THz pulse traces was used for signal analysis in the frequency domain, finding the spectrum of transmission coefficients, T_ω, defined as the squared ratio of Fourier harmonic amplitudes of sample and reference signals. More details about measurement setup can be found elsewhere [15], [27].

The transmission spectra of the sample F3 in the zone (2), i.e., initial heterostructure layers with conductive 2DEG layer, and in the zone (1), modified structure without 2DEG, are shown in Fig. 2. Both spectra demonstrate the Fabry–Perot (FP) fringes due to formation of standing waves in the sample. In case of F3(1), the period of FP oscillations was of $f_{\rm FP} = 94.2 \pm 0.2$ GHz. Taking dielectric permittivity as a constant, $\epsilon_s = 9.37$, the thickness of substrate with remaining layers was found to be of $D_s = 520 \pm 1$ μm, which was the same as physical thickness of the sample measured with a micrometer. Evidence of the 2DEG conductivity is seen in transmission spectrum below frequency of 1 THz as a monotonic suppression of magnitude and position small blue-shift of FP extrema [see sample F3(2)].

The transmission spectra of the sample F3 in zone (2) at two temperatures are shown in Fig. 3, by black square symbols. Detailed analysis of the spectra was performed using analytical expression of T_ω, derivation of which can be found

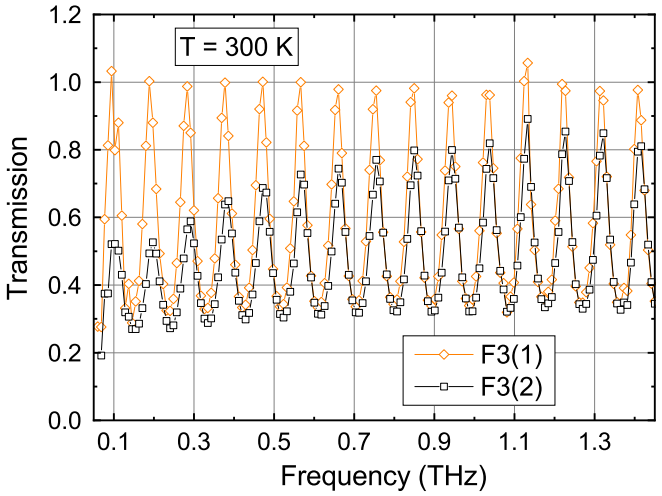

Fig. 2. Transmission spectra of different zones on the sample F3: zone F3(4) is with 2DEG layer, zone F3(1) is without 2DEG, where top layers were removed by the RIE methods. It is noted that thin lines connect the experimental points (symbols) for clarity purpose only.

elsewhere [16]

$$T_\omega = \left|\left[\cos(\psi_s) - i\frac{\epsilon_s+1}{2\sqrt{\epsilon_s}}\sin(\psi_s)\right] + \frac{\Gamma_e}{\gamma_e - i\omega} \times \left[\cos(\psi_s) - \frac{i}{\sqrt{\epsilon_s}}\sin(\psi_s)\right]\right|^{-2} \quad (2)$$

where ψ_s stands for $\psi_s = \sqrt{\epsilon_s}k_0 D_s$, $k_0 = \omega/c$ is wavenumber of the incident wave with angular frequency, $\omega = 2\pi f$, the light velocity in vacuum, $c = 3\times10^{10}$ cm/s, and the dielectric permittivity, $\epsilon_s = 9.37$. Parameters $\Gamma_e = 2\pi e^2/c \times n_e/m^*$ and $\gamma_e = 1/\tau_{sc}$ are the radiative and nonradiative decay rates, discussed in Section I. We would like to point out, that we made assumption about the ϵ_s independence on temperature based on the additional experiments investigating the optical performance of the nonconductive heterostructure layers and the substrate, the results of which were published elsewhere [15].

The calculated spectra are shown in Fig. 3 by black solid lines. The best fitting parameters for F3(2) sample at $D_s = 520 \pm 1$ μm were found to be $\Gamma_e = 1.92 \pm 0.02$ THz, $\gamma_e = 0.45 \pm 0.01$ THz at 80 K and $\Gamma_e = 1.32 \pm 0.15$ THz, $\gamma_e = 3.28 \pm 0.51$ THz at 300 K. It is worth to note the decrease of radiative decay rate value with the increase of temperature, which is unusual for semiconductors, if one assumes only the variation of 2DEG density which, according to the Hall experiment data, increased with temperature by 10% (see Table I) or remained unchanged for some heterostructures under investigation. Therefore, the thermal renormalization of the electron effective mass needs to be taken into account when evaluating the 2DEG density from the analysis of THz transmission spectra based on Drude conductivity model. To estimate the 2DEG density, we used values of $m^* = 0.22m_e$ at 80 K and $m^* = 0.34m_e$ at 300 K [19]. The results are summarized in the column "THz TDS" in Table I. The noncontact measurements of 2DEG parameters agree well

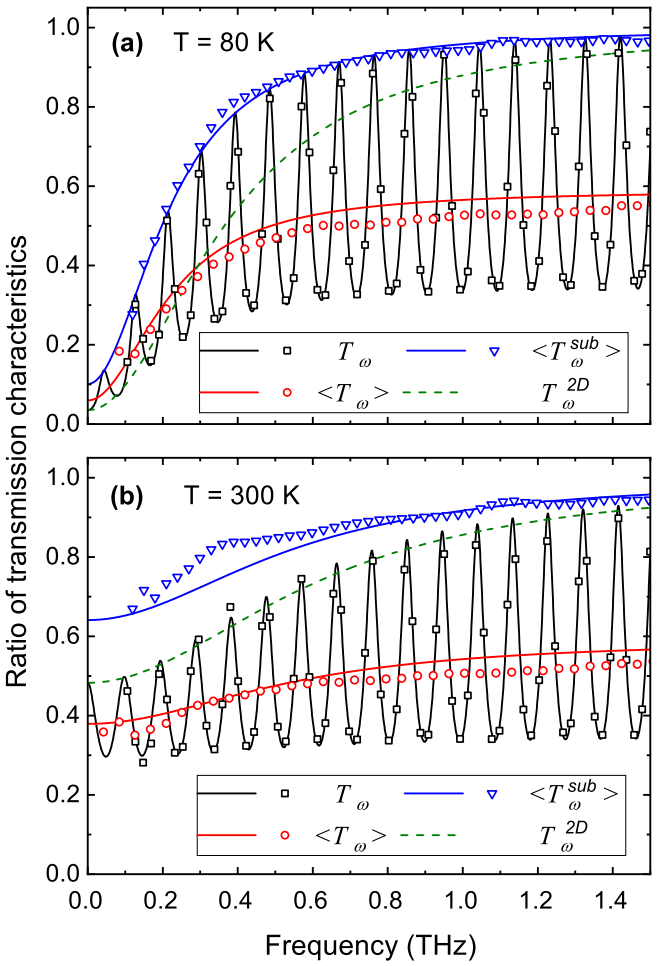

Fig. 3. Measured (symbols) and calculated (lines) transmission characteristics of the F3 sample at two temperatures of (a) 80 K and (b) 300 K. Data in black, red, and blue colors stand for spectra of T_ω, $\langle T_\omega \rangle$, and $\langle T_\omega^{sub} \rangle$, respectively. Green dashed lines demonstrate the transmission spectra of the free-standing 2DEG layer calculated using respective values of parameters found for F3 sample.

with the results of independent Hall experiment within an uncertainty of 10%.

Low resolution transmission spectra, $\langle T_\omega \rangle$, were found taking into account a short-time window of single-pass THz pulse without its multiple reflections inside the sample [27]. Low-resolution spectra for sample F3(2) are shown in Fig. 3 by red circle symbols. Corresponding spectrum numerically was found averaging (2) data with respect to the period of FP oscillations. The results are shown in Fig. 3, by red color lines. Spectra without FP oscillations appears as monotonic function possessing saturation at high-frequency range (>1 THz) where contribution of 2DEG conductivity is negligible. The shape of calculated spectra agree well with experiment except the difference in absolute transmission values which in latter case are smaller by about of 4% due to measurement peculiarities of single-pass THz pulses [15]. Such difference can be eliminated if one measures the ratio between a low-resolution transmission spectra obtained with respect to the air and to the substrate. In a case of F3 sample, it was realized by measuring the THz pulse transmission trough the zone F3(2), $\langle T_\omega^{F3(2)} \rangle$,

and F3(1) modified structure without 2DEG, $\langle T_\omega^{F3(1)}\rangle$, and calculating the ratio of $\langle T_\omega^{\text{sub}}\rangle = \langle T_\omega^{F3(2)}\rangle / \langle T_\omega^{F3(1)}\rangle$. The results are shown Fig. 3 by blue solid lines and triangle symbols. A very good agreement between absolute transmission values of experimental and numerical spectra without FP fringes was achieved.

The same approach was used to fit the experimental transmission spectra of other samples with AlN spacer. Best fit for sample C10 was found with $D_s = 520 \pm 1$ μm finding the high-frequency parameter values: $\Gamma_e = 2.34 \pm 0.08$ THz, $\gamma_e = 0.81 \pm 0.05$ THz at 80 K and $\Gamma_e = 1.58 \pm 0.16$ THz, $\gamma_e = 3.81 \pm 0.98$ THz at 300 K. Here again the decrease of radiative decay rate with the increase of temperature was found. The result confirms presence of the renormalization effect of electron effective mass in the AlGaN/AlN/GaN HEMT structures as it was observed previously employing more sophisticated approach [15]. Thus, detailed analysis of the THz transmission spectra, using appropriate knowledge of the sample properties, such as the thickness, 2DEG density, and mobility obtained in advance from independent experiments, revealed the dependence of electron effective mass on temperature in different HEMT structures.

It is worth to discuss the transmission spectrum, $T_\omega^{\text{2-D}}$, of the hypothetical free-standing 2DEG layer, which can be found from (2) when $D_s = 0$ μm

$$T_\omega^{\text{2-D}} = \frac{\omega^2 + \gamma_e^2}{\omega^2 + (\Gamma_e + \gamma_e)^2}. \tag{3}$$

The results are shown in Fig. 3, by green dashed lines. Calculated spectra at both temperatures differ significantly from those discussed above exhibiting different shape and absolute transmission values. For example, at higher frequencies, the $T_\omega^{\text{2-D}}$ characteristic tends to 1 similarly as $\langle T_\omega^{\text{sub}}\rangle$ while $\langle T_\omega\rangle$ saturates close to 0.5. Meanwhile, a behavior of all three characteristics is very different at lower frequencies at both temperatures.

Next, the ratio of transmission characteristics without FP features at selected two temperatures, $\langle t_\omega\rangle = \langle T_\omega\rangle(80\text{ K})/\langle T_\omega\rangle(300\text{ K})$, was analyzed. The results are shown in Fig. 4. The ratio of respective characteristics for the hypothetical free-standing 2DEG layer, $t_\omega^{\text{2-D}} = T_\omega^{\text{2-D}}(80\text{ K})/T_\omega^{\text{2-D}}(300\text{ K})$, is also presented by dashed line. In experiment, the magnitude of relative signals for all samples grows steadily up to the level of 1.0 with the increase of frequency in agreement with modeled characteristic under assumption that at 300-K temperature the effective mass is changed to $m^* = 0.34m_e$. If one would assume that effective mass does not dependent on temperature, then the relative spectrum would be a nonmonotonic function with a maximum at the frequency of about 0.5 THz (see dot-dashed line in Fig. 4). Modeled response of the free-standing 2DEG layer demonstrated a minor influence of the substrate to relative characteristics as shown in Fig. 4.

Finally, the ratio $\Gamma_e(80\text{ K})/\Gamma_e(300\text{ K})$ was proposed as the quantity to measure the renormalization effect, as the radiative decay rate is inversely proportional to effective mass. Note that it also depends on the 2DEG density which may vary with temperature even in nitride-based heterostructures. After

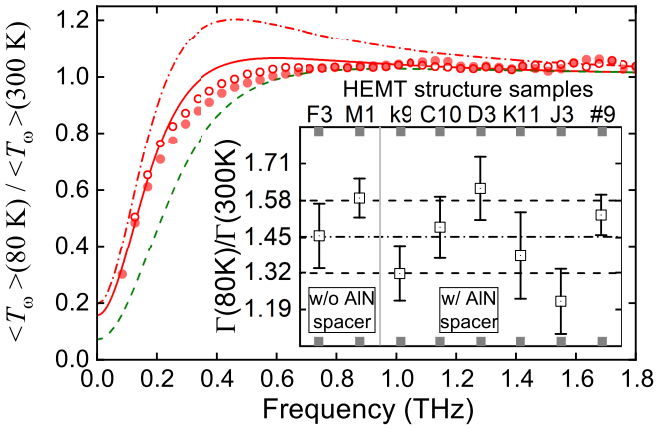

Fig. 4. Ratio of experimental characteristics of the selected samples: F3 (open symbols) and C10 (solid symbols). Modeled characteristics for respective parameter values of the F3 sample under assumption that the m^* at 300 K was of $0.22m_e$ (dot-dashed line) and $0.34m_e$ (solid line) and the same as latter but 2DEG without the substrate (dashed line). Inset: mean and standard deviation values of the radiative decay rate ratio for all heterostructures, as indicated, without and with AlN spacer between the AlGaN barrier and the GaN channel layers.

a number of measurement cycles of transmission spectra, size of $\Gamma_e(80\text{ K})/\Gamma_e(300\text{ K})$ was found to be of 1.45 ± 0.11 and 1.46 ± 0.13 for the samples F3 and C10, respectively. In a similar way the performance of 2DEG in all HEMT structures was investigates. The results of noncontact analysis are shown in the inset of Fig. 4. The renormalization of electron effective mass was observed in all HEMT samples without exception, demonstrating the average value of 1.45 ± 0.13. We note that some samples exhibited small increase of electron density with temperature, demonstrating change not larger than 10%, which were not included into analysis due to small value. Moreover, the results were in agreement with $0.34/0.22 = 1.55$ found from respective values of m^* previously reported in [18] and [19].

It is worth to point out that in this work the electron effective mass investigated in a frame of Drude model can be called as the optical effective mass the relationship of which with the transport effective mass and the effective mass of the density of states requires further research [13], [24].

III. Conclusion

The THz transmission spectra of AlGaN/(AlN)/GaN HEMT structures have been experimentally and numerically investigated at temperatures of 80 and 300 K. Found high-frequency response parameters of the 2DEG layer including electron density and mobility values were compared to the results of independent Hall measurements. Detailed analysis of the radiative decay rate revealed the increase of electron effective mass with temperature in all samples by a factor of 1.45 ± 0.13, indicating that the presence of AlN spacer between barrier and channel layers has no influence on this effect. The change of electron density with increase of temperature was observed for some samples however it was not taken into account because of smaller value. Thus, we proposed fast method for the phenomenon evaluation in the sample with thin Drude

conductivity layer and with weak carrier density dependence on temperature.

REFERENCES

[1] T. Palacios *et al.*, "High-power AlGaN/GaN HEMTs for Ka-band applications," *IEEE Electron Device Lett.*, vol. 26, no. 11, pp. 781–783, Nov. 2005, doi: 10.1109/LED.2005.857701.

[2] B. Romanczyk *et al.*, "W-band power performance of SiN-passivated N-polar GaN deep recess HEMTs," *IEEE Electron Device Lett.*, vol. 41, no. 3, pp. 349–352, Mar. 2020, doi: 10.1109/LED.2020.2967034.

[3] D.-Y. Chen *et al.*, "Microwave performance of 'buffer-free' GaN-on-SiC high electron mobility transistors," *IEEE Electron Device Lett.*, vol. 41, no. 6, pp. 828–831, Jun. 2020, doi: 10.1109/LED.2020.2988074.

[4] J. Jorudas *et al.*, "AlGaN/GaN on SiC devices without a GaN buffer layer: Electrical and noise characteristics," *Micromachines*, vol. 11, no. 12, p. 1131, Dec. 2020, doi: 10.3390/mi11121131.

[5] M. Bauer *et al.*, "A high-sensitivity AlGaN/GaN HEMT terahertz detector with integrated broadband bow-tie antenna," *IEEE Trans. THz Sci. Technol.*, vol. 9, no. 4, pp. 430–444, Jul. 2019, doi: 10.1109/TTHZ.2019.2917782.

[6] J. Sun *et al.*, "Passive terahertz imaging detectors based on antenna-coupled high-electron-mobility transistors," *Opt. Exp.*, vol. 28, no. 4, p. 4911, 2020, doi: 10.1364/OE.385042.

[7] M. S. Shur, "Terahertz plasmonic technology," *IEEE Sensors J.*, vol. 21, no. 11, pp. 12752–12763, Jun. 2021, doi: 10.1109/JSEN.2020.3022809.

[8] E.-S. Jang, M. W. Ryu, R. Patel, S. H. Ahn, K. J. Han, and K. R. Kim, "Performance enhancement of silicon-based sub-terahertz detector by highly localized plasmonic wave in nano-ring FET," *IEEE Electron Device Lett.*, vol. 42, no. 12, pp. 1719–1722, Dec. 2021, doi: 10.1109/LED.2021.3119926.

[9] S. Knight *et al.*, "*In-situ* terahertz optical Hall effect measurements of ambient effects on free charge carrier properties of epitaxial graphene," *Sci. Rep.*, vol. 7, no. 1, p. 5151, Dec. 2017, doi: 10.1038/s41598-017-05333-w.

[10] P. U. Jepsen, D. G. Cooke, and M. Koch, "Terahertz spectroscopy and imaging–modern techniques and applications," *Laser Photon. Rev.*, vol. 5, no. 1, pp. 124–166, Jan. 2011, doi: 10.1002/lpor.201000011.

[11] J. Horng *et al.*, "Drude conductivity of dirac fermions in graphene," *Phys. Rev. B, Condens. Matter*, vol. 83, no. 16, Apr. 2011, Art. no. 165113, doi: 10.1103/PhysRevB.83.165113.

[12] J. D. Buron *et al.*, "Graphene conductance uniformity mapping," *Nano Lett.*, vol. 12, no. 10, pp. 5074–5081, Oct. 2012, doi: 10.1021/nl301551a.

[13] E. D. Palik and J. K. Furdyna, "Infrared and microwave magnetoplasma effects in semiconductors," *Rep. Prog. Phys.*, vol. 33, p. 307, Sep. 1970, doi: 10.1088/0034-4885/33/3/307.

[14] S. Khorasani and B. Rashidian, "Modified transfer matrix method for conducting interfaces," *J. Opt. A, Pure Appl. Opt.*, vol. 4, no. 3, pp. 251–256, May 2002, doi: 10.1088/1464-4258/4/3/306.

[15] R. B. Adamov *et al.*, "Optical performance of two dimensional electron gas and GaN: C buffer layers in AlGaN/AlN/GaN heterostructures on SiC substrate," *Appl. Sci.*, vol. 11, no. 13, p. 6053, Jun. 2021, doi: 10.3390/app11136053.

[16] G. I. Syngayivska and V. V. Korotyeyev, "Electrical and highfrequency properties of compensated GaN under electron streaming conditions," *Ukrainian J. Phys.*, vol. 58, pp. 40–55, Jan. 2013, doi: 10.15407/ujpe58.01.0040.

[17] D. Pashnev, J. Jorudas, R. Balagula, A. Urbanowicz, and I. Kasalynas, "Investigation of THz transmission through semi-insulating substrate with a thin conductive layer," in *Proc. 46th Int. Conf. Infr., Millim. THz Waves (IRMMW-THz)*, Aug. 2021, pp. 1–2, doi: 10.1109/IRMMW-THz50926.2021.9567456.

[18] T. Hofmann *et al.*, "Temperature dependent effective mass in AlGaN/GaN high electron mobility transistor structures," *Appl. Phys. Lett.*, vol. 101, no. 19, Nov. 2012, Art. no. 192102, doi: 10.1063/1.4765351.

[19] D. Pashnev *et al.*, "Experimental evidence of temperature dependent effective mass in AlGaN/GaN heterostructures observed via THz spectroscopy of 2D plasmons," *Appl. Phys. Lett.*, vol. 117, no. 16, Oct. 2020, Art. no. 162101, doi: 10.1063/5.0022600.

[20] N. Armakavicius *et al.*, "Properties of two-dimensional electron gas in AlGaN/GaN HEMT structures determined by cavity-enhanced THz optical Hall effect," *Phys. Status Solidi C*, vol. 13, nos. 5–6, pp. 369–373, May 2016, doi: 10.1002/pssc.201510214.

[21] A. M. Kurakin *et al.*, "Quantum confinement effect on the effective mass in two-dimensional electron gas of AlGaN/GaN heterostructures," *J. Appl. Phys.*, vol. 105, no. 5, pp. 73703-1–73703-6, 2009.

[22] H. Morkoç, *Nitride Semiconductor Devices*. Weinheim, Germany: Wiley, Apr. 2013, doi: 10.1002/9783527649006.

[23] S. Schöche *et al.*, "Terahertz optical-Hall effect characterization of two-dimensional electron gas properties in AlGaN/GaN high electron mobility transistor structures," *Appl. Phys. Lett.*, vol. 98, no. 9, Feb. 2011, Art. no. 092103, doi: 10.1063/1.3556617.

[24] D. Tsui, S. Allen, R. Logan, A. Kamgar, and S. Coppersmith, "High frequency conductivity in silicon inversion layers: Drude relaxation, 2D plasmons and minigaps in a surface superlattice," *Surf. Sci.*, vol. 73, pp. 419–433, May 1978, doi: 10.1016/0039-6028(78)90520-4.

[25] S. A. Mikhailov, "Plasma instability and amplification of electromagnetic waves in low-dimensional electron systems," *Phys. Rev. B, Condens. Matter*, vol. 58, no. 3, pp. 1517–1532, Jul. 1998, doi: 10.1103/PhysRevB.58.1517.

[26] X. Wang, D. J. Hilton, L. Ren, D. M. Mittleman, J. Kono, and J. L. Reno, "Terahertz time-domain magnetospectroscopy of a high-mobility two-dimensional electron gas," *Opt. Lett.*, vol. 32, no. 13, p. 1845, Jul. 2007, doi: 10.1364/OL.32.001845.

[27] D. Pashnev *et al.*, "Terahertz time-domain spectroscopy of two-dimensional plasmons in AlGaN/GaN heterostructures," *Appl. Phys. Lett.*, vol. 117, no. 5, Aug. 2020, Art. no. 051105, doi: 10.1063/5.0014977.